Fast simulator of the electric sense for complex scene

M.Rédha Benachenhou*, Fréderic Boyer, Christine Chevallereau, Vincent Lebastard

***Abstract*— The aim of this paper is to extend the analytical model of a sensor for the navigation of underwater vehicles by electric sense to the complex scene and to develop a simulator based on this model that should be fast and accurate.**

I. Introduction

The perception of aquatic surroundings is essential for the enhancement of safety and trajectory-control systems of underwater robots, but the perception in troubled and dark waters are not easy, in this case the classical approaches like cameras or sonar are inadequate. The perception method applied here is bio-inspired from the electric sense electrolocation discovered in the 50s by H.W. Lissman [1].

II. Sensor

III. Model of the electric response to a single small object

We here reconsider the modeling approach of [2], whose the purpose was to predict the electric interactions between a slender active agent with a single small object. This model allows one to derive a simple analytical expression of the measurements induced by the presence of the object. We here start from this result, and extend it to the case where the electric measurements of the sensor are induced by other perturbative primitives as a wall or a corner. This kind of scenes, which contains only one primitive are named simple scenes and distinguished from the complex scenes where the sensor simultaneously senses the presence of several small objects. Going further, in a second step, we will then extend this result to the case of scenarios involving several agents, some of them being active while other are passive. At the end, we will propose a fast simulator able to simulate electric interactions between as set of slender agents navigating in an insulating tank where objects are immersed. In all the following, A denotes one of these agents (today a robot, in future, a robot). As previously stated, such a sensor will be modeled as an axi-symmetrical probe whose the insulating boundaries will be covered of $m+1$ conductive rings $\mathcal{E}_\alpha$, or electrodes denoted $\mathcal{E}_{\alpha=0,1...m}$. Except $\mathcal{E}_0$ which is connected, all the $\mathcal{E}_\alpha$ are divided into an even number of identical electrically independent angular sectors two by two opposed. We shall denote by $n+1$, the total of all independent sectors of these rings with $\cup_{\alpha=0}^{m}\mathcal{E}_\alpha = \cup_{k=0}^{n} e_k$. While we polarize the $\mathcal{E}_\alpha$ with respect to the ground electrode $\mathcal{E}_0$ with imposed voltages U_α, we measure the currents I_k crossing the e_k for $k = 1, 2...n$. By convention $\mathbf{x}_\alpha$ will refer to the center of the ring $\mathcal{E}_\alpha$.

In [2], we have shown that the vector $\mathbf{I}$ of the measured currents in the presence of a (small) perturbative object in the scene, can be reasonably developed as the following superimposition of three components:

$$\mathbf{I} = \mathbf{I}^{(0)} + \mathbf{I}^{(1)} + \mathbf{I}^{(2)} + O(\epsilon^\kappa). \quad (1)$$

Each of these contributions is a vector of dimension $((n+1)\times 1)$ that contains the currents which cross the e_i, where the small amount ϵ is a feature of the problem. Typically in this case, ϵ is the aspect ratio (R/l) of the slender sensor with R its radius and l, its length. Equivalently, ϵ is the ratio a/r where a is the dimension of the object and r, the distance between the sensor and the object. From left to right we find in , the vector of basal currents, i.e. the currents which would be measured when there is not any object close to the object (*step 0* of Fig.2). The second component, $\mathbf{I}^{(1)}$ represents the vector of the currents reflected by the object while the sensor is absent in the scene (*step 1* of Fig.2), while $\mathbf{I}^{(2)}$ represents the reaction of the sensor to the excitation $\mathbf{I}^{(1)}$. Note that it is thanks to $\mathbf{I}^{(2)}$, that the sensor can recover its electric balance (in *step 2* of Fig.2).

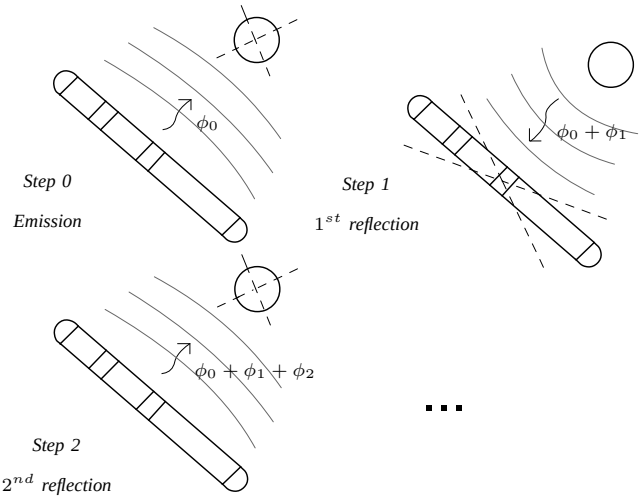

Fig. 1. The method of the successive reflections. First step (top left): we ignore the object and we solve the Laplace equation for ϕ_0. Second step (top right): this time we ignore the sensor and we solve the Laplace equation for $\phi_0 + \phi_1$ where ϕ_1 is the perturbation of ϕ_0 induced by the object. Third step (bottom left): we solve the Laplace equation for $\phi_0 + \phi_1 + \phi_2$ ignoring the object this time, ϕ_2 being the perturbation of $\phi_0 + \phi_1$. Each novel potential field can be represented as a new contribution (to ϕ) reflected by the object or the sensor.

To this first decomposition of the total currents vector we can add another one which is based on the morphology of the sensor. Indeed, thanks to the symmetries of the sensor, the vector of total currents can be decomposed as a sum of two

components named *"lateral currents"* and *"axial currents"* as follows:

$$\mathbf{I} = \mathbf{I}_{ax} \oplus \mathbf{I}_{lat}. \quad (2)$$

In (2), $\mathbf{I}_{ax}$ is axi-symmetric whereas the component $\mathbf{I}_{lat}$ is axi-skewsymmetric (Fig. 1). In other words, for any of the e_i belonging to a same $\mathcal{E}_\alpha$, the components $I_{ax,i}$ are identical whereas for a couple of opposed (e_i, e_{i+1}) on a same ring $\mathcal{E}_\alpha$, we have $I_{lat,i} = -I_{lat,i+1}$. From these considerations, it is easy to extract $\mathbf{I}_{lat}$ and $\mathbf{I}_{ax}$ from $\mathbf{I}$ using the relations:

$$\mathbf{I}_{ax} = \mathbf{D}_+\mathbf{P}_+\mathbf{I}, \ \mathbf{I}_{lat} = \mathbf{I} - \mathbf{I}_{ax} \quad (3)$$

Where $\mathbf{P}_+$ projects the currents crossing the e_k on those crossing the $\mathcal{E}_\alpha$, by simply adding all the I_k of a same ring $\mathcal{E}_\alpha$, that being done ring by ring. Regarding $\mathbf{D}_+$, it is the $(n+1)\times(m+1)$ matrix defined by $D_{+(i\alpha)} = A_i/A_\alpha$ if $e_i \subset \mathcal{E}_\alpha$ and $D_{+(i\alpha)} = 0$ otherwise, with A_i and A_α the area of e_i and $\mathcal{E}_\alpha$ respectively. This matrix allows one to equi-distribute the I_α onto the e_k with $e_k \in \mathcal{E}_\alpha$. With these definitions, we associate to any vector $\mathbf{I}$ the vector of the reduced currents $\overline{\mathbf{I}}$, by the relation:

$$\overline{\mathbf{I}} = \mathbf{P}_+\mathbf{I} \quad (4)$$

Moreover, $\mathbf{I} = \mathbf{I}^{(0)}$ is axi-symmetric since there is no object around the sensor to break the symmetry of the scene, and because the boundaries of the sensor and the boundary conditions imposed on them are also axi-symmetric. Moreover, the base currents vector $\overline{\mathbf{I}}^{(0)}$ is linked to the vector of imposed voltages by the axial conductance matrix :

$$\overline{\mathbf{I}}^{(\mathbf{0})} = \overline{\mathbf{C}}^{(0)}\mathbf{U}, \quad (5)$$

with $\mathbf{U}$ the vector of voltages on the rings and $\overline{\mathbf{C}}^{(\mathbf{0})}$ is the $(m+1)\times(m+1)$ conductance matrix. Now, by the combining the two previous decompositions (III) and (2), we find :

$$\mathbf{I}_{lat} = \mathbf{I}^{(0)}_{lat} + \mathbf{I}^{(1)}_{lat} + \mathbf{I}^{(2)}_{lat} \ , \ \mathbf{I}_{ax} = \mathbf{I}^{(0)}_{ax} + \mathbf{I}^{(1)}_{ax} + \mathbf{I}^{(2)}_{ax}. \quad (6)$$

From the previous considerations, we have $\mathbf{I}^{(0)}_{lat} = 0$, whereas $\mathbf{I}^{(1)}_{lat}$ is merely the lateral flux of the first reflection electric field through the measurement electrodes, i.e.:

$$\mathbf{I}^{(1)}_{lat} = -\left(\int_{e_0} \boldsymbol{\nabla}\phi_1.\mathbf{n}_\perp ds, ..., \int_{e_n} \boldsymbol{\nabla}\phi_1.\mathbf{n}_\perp ds\right)^T. \quad (7)$$

Going further, $\mathbf{I}^{(2)}_{lat} = \mathbf{S}_\perp\mathbf{I}^{(1)}_{lat}$ with $\mathbf{S}_\perp$ a diagonal matrix whose coefficients are positive constants on each $\mathcal{E}_\alpha$ since they model the reinforcement of $\mathbf{I}^{(1)}_{lat}$ due to the lateral polarization of the $\mathcal{E}_\alpha$ and the funneling of the current lines towards the electrodes by their insulating contiguous boundaries. From these first considerations we deduce the model of the lateral currents as following:

$$\mathbf{I}_{lat} = (\mathbf{1} + \mathbf{S}_\perp)\mathbf{I}^{(1)}_{lat}, \quad (8)$$

with $\mathbf{1}$, the identity matrix. Regarding the axial currents, $\mathbf{I}^{(0)}_{ax} = \mathbf{I}^{(0)}$, $\mathbf{I}^{(1)}_{ax} + \mathbf{I}^{(2)}_{ax}$ represents the axial response of the sensor to the potential field reflected by the primitive [2]. This field is applied on each of the rings $\mathcal{E}_\alpha$. Going further, due to the smallness of electrodes with respect to the potential variations, the potential field can be expanded on each $\mathcal{E}_\alpha$ as:

$$\phi_1(\mathbf{x}) \simeq \phi_1(\mathbf{x}_\alpha) + \nabla\phi_1(\mathbf{x}_\alpha).(\mathbf{x} - \mathbf{x}_\alpha) \quad (9)$$

As a result, the axial response of the sensor has two components, one for each of the components of (9). The leading order one, $\mathbf{I}^{(2)}_{ax}$, is the response of the sensor to the axial polarization by the vector of iso-potentials $\Phi_1 = (\phi_1(\mathbf{x}_{c0}), ...\phi_1(\mathbf{x}_{cm}))^T$. The second, $\mathbf{I}^{(1)}_{ax}$, represents the axial polarization of the rings by the reflected electric field $-\nabla\phi_1$. It has one order of magnitude more than $\mathbf{I}^{(2)}_{ax}$ [2]. But since the response of the sensor consists in compensating the incident potentials of Φ_1 through the generation of a vector of additional potentials on its electrodes: $\Phi_2 = -\Phi_1$, the perturbative component of axial currents can be written at the leading order as:

$$\mathbf{I}_{ax} - \mathbf{I}^{(0)} \simeq \mathbf{I}^{(2)}_{ax} = \mathbf{D}_+(-\overline{\mathbf{C}}^{(0)}\Phi_1), \quad (10)$$

In [2] we have showed that only $\mathbf{I}^{(1)}_{lat}$ and Φ_1 depend on the object through the relations :

$$\mathbf{I}^{(1)}_{lat} = \mathbf{L}\overline{\mathbf{I}}^{(0)}, \quad \Phi_1 = \mathbf{K}\overline{\mathbf{I}}^{(0)}, \quad (11)$$

where $\mathbf{L}$ and $\mathbf{K}$ are two matrices depending on the geometry of the object and its situation (position orientation) relatively to the sensor. Finally, inserting (11) in (10), (6) can be written at the end:

$$\mathbf{I}_{lat} = (\mathbf{1} + \mathbf{S}_\perp)\mathbf{L}\overline{\mathbf{I}}^{(0)} \ , \ \mathbf{I}_{ax} = \mathbf{D}_+(\mathbf{1} - \overline{\mathbf{C}}^{(0)}\mathbf{K})\overline{\mathbf{I}}^{(0)}. \quad (12)$$

In fact, the previous context can be extended from a single small object to other primitives including:

- A wall
- An agent

In the following, we first consider the case where only one of these primitives is present in the sensor surroundings. In this case, we will refer to "simple scenes" that we will oppose later to "complex scenes" where several primitives interact around the sensor.

IV. Application to simple scenes

To calculate the axial and lateral currents in simple scenes, it suffices to calculate the "sensor response" matrices $\mathbf{L}$ and $\mathbf{K}$ to each of the primitives. Indeed, the complete model is then completely known since $\overline{\mathbf{I}}^{(0)}$ and $\overline{\mathbf{C}}^{(0)}$ can be directly measured on the sensor in a preliminary calibration phase. In order to prepare the case of complex scenes, in what follows the matrices $\mathbf{L}_{X/Y/Z}$, $\mathbf{K}_{X/Y/Z}$ are the previously defined matrices of interaction, where X, Z represents the agents by which the signal begins and end respectively and Y is the primitive by which the signal passes in transit. Since in the case of simple scene, only one agent is concerned we will necessarily have in this section $X = Z$.

1) Particular case of a small object: For an object centered on $\mathbf{y}_c$ and by setting $\mathbf{y}_c - \mathbf{x}_{c\alpha} = \mathbf{r}_\alpha$, we define a function $f_{e\mathcal{E}}$ that associates to any i corresponding to the index of an electrode e_i, the index α of the ring $(\mathcal{E}_\alpha)$ to which it belongs : $\alpha = f_{e\mathcal{E}}(i)$. In agreement with the reflections method, the electric interactions are represented by reflections traveling between the primitives of the scene. As a result, it is practical to represent these interactions in the form of a graph whose nodes are the primitives by which the signals pass in transit, and vertices are the travel paths. As a first illustration, Fig 2.b shows the graph of interactions in the case of a single object. In this case, the signal goes from the sensor (A) to the object (O) before coming back to A. As regards the first travel, it is shown in [2] that for any $\mathbf{x}$ in the sensor surroundings, we have:

$$\phi_0(\mathbf{x}) = \frac{1}{4\pi} \sum_{\alpha=0}^{m} \frac{\overline{I}_\alpha^{(0)}}{\gamma \|\mathbf{r}_\alpha\|} + O(\epsilon) \tag{13}$$

while for the second travel we have:

$$\phi_1(\mathbf{x}) = -\frac{\mathbf{r}.\mathbf{P}.\nabla\phi_0}{\| \mathbf{r} \|^3}\ , \tag{14}$$

Now inserting (13) in (14) and the result in (7) and the vector of potentials $\Phi_1 = (\phi_1(\mathbf{x}_{c0}), ...\phi_1(\mathbf{x}_{cm}))^T$ allows to obtain by identification with (11), the two response matrices as (with $\alpha = f_{e\mathcal{E}}(i)$):

$$\mathbf{L} = \mathbf{L}_{A/O/A} = (L_{i,\beta})_{1\leq i\leq n+1, 1\leq\alpha\leq m+1} \tag{15}$$

$$L_{i,\beta} = -\frac{\overline{A_i}}{4\pi\|\mathbf{r}_\alpha\|^3}(2\cos(\nu_i)\mathbf{e}_{r,\alpha} - \cos(\mu_i)\mathbf{e}_{\theta,\alpha}).\mathbf{P}.\frac{\mathbf{r}_\beta}{\|\mathbf{r}_\beta\|^3},$$

and:

$$\mathbf{K} = \mathbf{K}_{A/O/A} = (K_{\alpha,\beta})_{1\leq\alpha,\beta\leq m+1}$$

$$K_{\alpha,\beta} = -\frac{1}{4\pi\gamma}\frac{\mathbf{r}_\alpha.\mathbf{P}.\mathbf{r}_\beta}{\|\mathbf{r}_\alpha\|^3\|\mathbf{r}_\beta\|^3}. \tag{16}$$

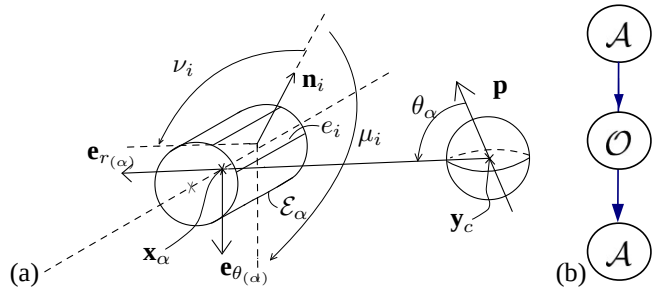

Fig. 2. (a) A sheme of perturbated ϵ_α of the sensor is depicted, $\mathbf{n}_i$ is the normal vector to e_i in the local farm $(\mathbf{e}_r, \mathbf{e}_\theta, \mathbf{e}_\phi)(\mathbf{x}_{c\alpha})$ associated to the spherical coordinates centered on the object and such as $\cos(\nu_i) = \mathbf{n}_i.\mathbf{e}_{r_{(\alpha)}}$, $\cos(\mu_i) = \mathbf{n}_i.\mathbf{e}_{\theta_{(\alpha)}}$, $\cos(\theta_\alpha) = \mathbf{e}_3.\mathbf{e}_{r_{(\alpha)}}$ with $\mathbf{e}_{r_{(\alpha)}} = \mathbf{r}_\alpha/\|\mathbf{r}_\alpha\|$,$\mathbf{e}_3 = \mathbf{p}/\|\mathbf{p}\|$, $\mathbf{p} = \mathbf{P}.\mathbf{E}_0$, $\mathbf{e}_{\theta_{(\alpha)}} = ((\mathbf{e}_3 \times \mathbf{e}_{r_{(\alpha)}}) \times \mathbf{e}_{r_{(\alpha)}})/\sin(\theta_\alpha)$ and $\mathbf{E}_0$ is the electric field on the object center. (b) Graphical representation of the contribution of the sphere O on the sensor A. There is just one passage through the object and we write $A/O/A$.

Where all the notations related to the geometry of the scene and the sensor are shown in (Fig.2 a), while γ is the electrical conductivity of the medium, and $\overline{A_i}$ is the apparent area offered by the sector e_i to the signal reflected by the object with :

$$\overline{A_i} = sinc\left(\frac{\lambda_i}{2}\right) A_i, \tag{17}$$

where $sinc$ denotes the cardinal sinus function such that $sinc(x) = \frac{\sin(x)}{x}$, λ_i is the azimuthal aperture of the angular sector e_i, while A_i is the area of sector e_i. In (16) and (16), the intrinsic properties of the object are encoded in a unique tensor, named the polarization tensor of the object and here denoted $\mathbf{P}$. In the particular case where the object is spherical $\mathbf{P} = \chi a^3 \mathbf{1}$, where $\mathbf{1}$ is the identity tensor and a the radius of the sphere while $\chi = (\gamma_1 - \gamma)/(2\gamma - \gamma_1)$ is the contrast factor between the two materials composing the scene, i.e. the water of conductivity γ and the object O of conductivity γ_1. Finally, returning to (1) and (6), an expansion in perturbations detailed in [2] has shown that we have in the case of a small object, for the axial currents: $\mathbf{I}_{ax} = \mathbf{I}_{ax}^{(0)} + \mathbf{I}_{ax}^{(2)} + O(\epsilon^\kappa)$ with $\kappa = 4$, while for the lateral current $\mathbf{I}_{lat} = \mathbf{I}_{lat}^{(1)} + \mathbf{I}_{lat}^{(2)} + O(\epsilon^\kappa)$, with $\kappa = 5$.

si je suis isolant, -1/2. Si c'est un conducteur, xi = 1

A. Particular case of large objects (insulating flat wall)

For the wall we use the method of image charges [3]. According to this method, to model the influence of an insulating plan, a virtual sensor identical to the real one, named image, is placed symmetrically with respect to the plane. This artifice allows one to superimpose to the real electric field, that of its image, and due to the symmetry the total field does satisfy the boundaries conditions imposed by the wall (it is tangent to the wall). As in the case of an object, ϕ_0 denotes the potential produced by the sensor in absence of wall when it is submitted to the voltages vector $\mathbf{U}$ and ϕ_1 represents the potential in any point of space reflected by the wall. As a result, ϕ_1 must be calculated so as $\phi_0 + \phi_1$ satisfies the boundary conditions on the insulating wall, i.e. on any point of this wall, we shall have:

$$\frac{\partial\phi_0}{\partial n} = -\frac{\partial\phi_1}{\partial n} \tag{18}$$

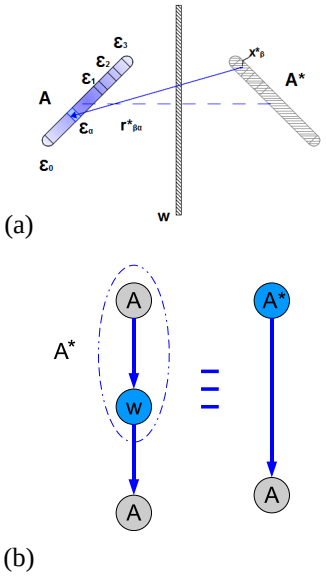

Fig. 3. (a) A^* is the virtual sensor symetrical of the real one A to the wall W. (b) Graphical representation of the contribution of the image sensor A^* on the sensor A. There is just one passage through the wall and we write $A/W/A = A^*/A$.

Now replacing the wall by the symmetric image A^* of the sensor A with respect to the wall boundaries (see Fig. IV-A), the potential ϕ_1 received by A is the potential produced by the virtual agent A^* while the real one is removed from the scene, i.e.:

$$\phi_1(\mathbf{x}) = \frac{1}{4\pi\gamma} \sum_{\beta=1}^{m+1} \frac{\overline{I}_\beta^{(0)}}{\|\mathbf{r}_\beta^*(\mathbf{x})\|}, \tag{19}$$

with $\mathbf{r}_\beta^*(\mathbf{x}) = \mathbf{x} - \mathbf{x}_{c\beta}^*$ where $\mathbf{x}$ is the position in which ϕ_1 is evaluated and $\mathbf{x}_{c\beta}^*$ is the center of the ring β of the image sensor A^*. Let us note that the basal currents of (19) are those of the real sensor since its image is in the same electric state. Now, using the expression (19) of ϕ_1 in (7) and the vector of potentials $\Phi_1 = (\phi_1(\mathbf{x}_{c0}), ...\phi_1(\mathbf{x}_{cm}))^T$ allows to obtain by identification with (11), the two response matrices ($\mathbf{K}_{A^*/A} = (K_{\alpha,\beta})$ and $\mathbf{L}_{A^*/A} = (L_{i,\beta})$) of the sensor to a wall:

$$K_{\alpha,\beta} = \frac{1}{4\pi\gamma\|\mathbf{r}_{\beta\alpha}^*\|} \ , \ L_{i,\beta} = \frac{\overline{A_i}\mathbf{r}_{\beta\alpha}^*.\mathbf{n}_i}{4\pi\|\mathbf{r}_{\beta\alpha}^*\|^3}, \tag{20}$$

where $\mathbf{r}_{\beta\alpha}^* = \mathbf{x}_{c\alpha} - \mathbf{x}_{c\beta}^*$ and $\alpha = f_e\mathcal{E}(i)$. Finally, referring to (1) and (6) the second reflection approximation of the axial currents, gives for a wall $\mathbf{I}_{ax} = \mathbf{I}_{ax}^{(0)} + \mathbf{I}_{ax}^{(2)} + O(\epsilon^\kappa)$ with $\kappa = 1$ and $\epsilon = (R/r^*)$ and r^*, the distance between the center of the sensor and that of its image. For the lateral current, we have $\mathbf{I}_{lat} = \mathbf{I}_{lat}^{(1)} + \mathbf{I}_{lat}^{(2)} + O(\epsilon^\kappa)$, with $\kappa = 2$.

B. Extension to insulating corners

In the following, we also consider the case where the primitives are two and three dimensional corners. In the first case, the corner is the result of the intersection of two orthogonal planes, while in the second case, three orthogonal planes intersect into a single vertex. Thus it is easy to combine the response of a single wall to build that of these two kinds of corner. In the 2D-corner we just have to superimpose the response of the two planar symmetric images with respect to the two walls with a third image, properly related to the corner and deduced by symmetrizing the two wall images with respect to the two planes prolonged beyond their material boundaries (see Fig.4). Finally, since a 3D-corner is formed by 3 2D-corners and a point vertex, the first reflected potential is generated by $3 \times 3 = 9$ images of the previous (2D-corner) type, plus one image properly due to the 3D-corner and obtained by applying a central symmetry with respect to the point vertex to the real agent. Finally, all these considerations correspond to add several times the wall response matrices K and L of (19) with the appropriate configurations of the mirror image of the sensor.

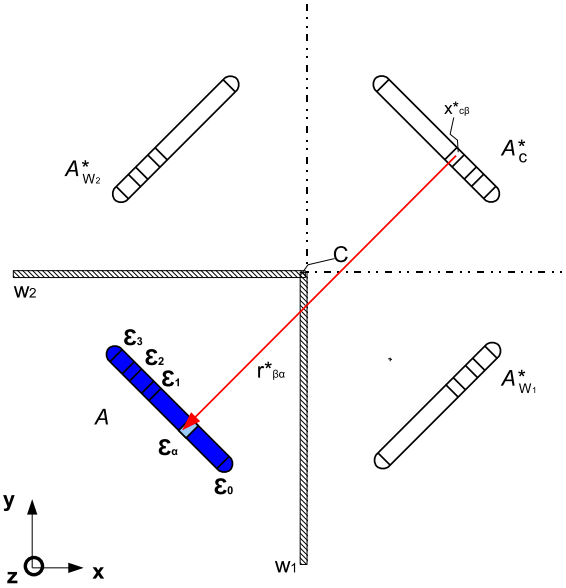

Fig. 4. $A_{w_1}^*$, $A_{w_2}^*$ are the virtual sensors symetrical of the real one A to the wall w_1 and w_2 respectively and A_c^* is the virtual sensor symetrical of the real one A to the corner C.

V. Complex scenes

A complex scene is a set of several primitives electrically interacting simultaneously.

1) General treatment: In order to cope with multiple primitives. We visualize the different reflections which travel from primitive to primitive in the form of a graph as previously introduced. For instance in the case where the sensor is surrounded by two small objects or a wall and an objet, we can represent the electric interactions as a graph (said "of reflections") constituted of 3 nodes and 3 branches. Now, when the agent emit a signal, just imagine that it travels from node to node with a possibility of going forward to the next node or to come backward to the previous one and so on... With the increasing number of

travels a quasi-steady regime arises in a very short transitory time.

2) Rules of approximation: We have now at our disposal all the results required to assess the order of accuracy of our approximation. As regards the potentials, combining (13) and (5), and because $\overline{C}^{(0)}\gamma^{-1} = O(R)$ (see [2]), it appears that, reflection after reflection, when the signal passes the sensor it decreases by a factor $\varepsilon = R/r$ (i.e. of one order of magnitude). On the other hand, comparing (13) and (14) shows that when the signal passes in transit by the object, it is attenuated by a factor of order ε^3 (i.e. of 3 orders). Also, we have $|\phi_0/U| = |\phi_2/\phi_1| = O(\varepsilon)$ while $|\phi_1/\phi_0| = O(\varepsilon^3)$. Inspecting the currents is even more simple since it suffices to consider (10-12) to find, with from (16,16) $L = O(\varepsilon^5)$ and $\gamma K = O(\varepsilon^4)$: $|I^{(1)}/I^{(0)}| = O(\varepsilon^5)$ and $|I^{(2)}/I^{(0)}| = O(\varepsilon^4)$. Finally, in the case of an insulating wall, since the wall reflects all the incident energy, the wall does not introduce any attenuation. This is shown by a direct computation of $|\phi_1/\phi_0|$ with (13) and (19) or by remarking that the reflected potential is that emitted by an ubiquitous image of the sensor. In the same manner than for a small object, considering (20) we find $K = O(\varepsilon)$ and $L = O(\varepsilon^2)$, and so: $|I^{(1)}/I^{(0)}| = O(\varepsilon^2)$ and $|I^{(2)}/I^{(0)}| = O(\varepsilon)$.
From these considerations we deduce the following rules of approximation. In fact, in order to trunk the expansion generated by the successive reflections, we first have to fix a given order of approximation. Then we push the expansion in a consistent manner by including more and more reflections in the model till to capture all the terms of the fixed order. In order to fix the order of the expansion we decided to retain the minimum order at which the smallest primitive appears in the measurements. This criterium is in fact quite natural since it corresponds to fix the resolution of the method. This rules can be easily checked on the graph of interactions by adding two remarks. First, the attenuation factors of the currents are of those of order as those of the traveling potential ...

3) scene with a wall and a sphere (small object): In the case of a complex scene, we will superimpose the responses from objects and their mutual influences and obtain a model of the disturbance current consistent with the order where there is minimal disturbance of less than the seeks to capture, e.i. that of a small isolated object. From the image method [3] we know that the electric field is tangential to the wall involving a symmetry of the electric field vector for objects and their images, we deduced that the vector of the applied field $\vec{\mathbf{E}}_0$ for small object O and $\vec{\mathbf{E}^*}_{0_w}$ applied on the image to the wall O_w^* are symmetrical. As the field is based on the distances then the currents depend only on the geometry of objects in the scene. We decompose the interactions in this scene as shown in the Fig. 5 (a), all these interactions are referred on the sensor (e.i. measures are upon him).

We deduce that for one passage through objects there are 5 interactions who play a role in this tree, the equations are written:

$$\overline{\mathbf{I}}^{(\mathbf{2})}_{\mathbf{ax}} = -\overline{\mathbf{C}}^{(0)}\mathbf{K}\overline{\mathbf{I}}^{(\mathbf{0})} \tag{21}$$

with :

$$\mathbf{K} = \mathbf{K}_{A_w^*/A} + \mathbf{K}_{A/O/A} + \mathbf{K}_{A/O_w^*/A} + \mathbf{K}_{A_w^*/O/A} + \mathbf{K}_{A_w^*/O_w^*/A} \tag{22}$$

Where:

- The first term describes the effect of the image A_w^* on the sensor A. $\mathbf{K}_{A_w^*/A}$ is given in (20).
- The second term describes the effect of the sphere O on the sensor A. $\mathbf{K}_{A/O/A}$ is given in (16).
- The third term describes the effect of the image of the sphere O_w^* on the sensor A. $\mathbf{K}_{A/O_w^*/A}$ is given in (16) with $\vec{r_\alpha} = y_c^* - x_{c\alpha}$ and $\vec{r_\beta} = y_c^* - x_{c\beta}$.
- The fourth term describe the effects of the image sensor to the wall A_w^* on the sphere O. $\mathbf{K}_{A_w^*/O/A}$ is given in (16) with $\vec{r_\alpha} = y_c - x_{c\alpha}$ and $\vec{r_\beta} = y_c - x_{c\beta}^*$.
- The fifth term describe the effects of the image sensor to the wall A_w^* on the image of the sphere O_w^*. $\mathbf{K}_{A_w^*/O_w^*/A}$ are given in (16) with $\vec{r_\alpha} = y_c^* - x_{c\alpha}$ and $\vec{r_\beta} = y_c^* - x_{c\beta}^*$.

The same thing for the lateral :

$$\mathbf{I}^{(\mathbf{1})}_{\mathbf{lat}} = \mathbf{L}\overline{\mathbf{I}}^{(\mathbf{0})} \tag{23}$$

With:

$$\mathbf{L} = \mathbf{L}_{A_w^*/A} + \mathbf{L}_{A/O/A} + \mathbf{L}_{A/O_w^*/A} + \mathbf{L}_{A_w^*/O/A} + \mathbf{L}_{A_w^*/O_w^*/A} \tag{24}$$

Note here that if we want to go further in the order of approximation, we must go further in the reflection method and make back and forth between the sensor and the objects. Thus, for the following back and forth $\mathbf{I^{(2)}}$ takes the place of $\mathbf{I^{(0)}}$, $\mathbf{I^{(3)}}$ of $\mathbf{I^{(1)}}$ and $\mathbf{I^{(4)}}$ of $\mathbf{I^{(2)}}$, then:

$$\begin{aligned}
\overline{\mathbf{I}}^{(\mathbf{4})}_{\mathbf{ax}} &= -\overline{\mathbf{C}}^{(0)}\mathbf{K}\overline{\mathbf{I}}^{(\mathbf{2})}_{\mathbf{ax}} \\
\overline{\mathbf{I}}^{(\mathbf{6})}_{\mathbf{ax}} &= -\overline{\mathbf{C}}^{(0)}\mathbf{K}\overline{\mathbf{I}}^{(\mathbf{4})}_{\mathbf{ax}} \\
\overline{\mathbf{I}}^{(\mathbf{8})}_{\mathbf{ax}} &= -\overline{\mathbf{C}}^{(0)}\mathbf{K}\overline{\mathbf{I}}^{(\mathbf{6})}_{\mathbf{ax}} \\
&\vdots,
\end{aligned} \tag{25}$$

with:

$$\overline{\mathbf{I}}_{\mathbf{ax}} = \overline{\mathbf{I}}^{(\mathbf{0})}_{\mathbf{ax}} + \overline{\mathbf{I}}^{(\mathbf{2})}_{\mathbf{ax}} + \overline{\mathbf{I}}^{(\mathbf{4})}_{\mathbf{ax}} + \dots \tag{26}$$

and

$$\begin{aligned}
\mathbf{I}^{(\mathbf{3})}_{\mathbf{lat}} &= \mathbf{L}\overline{\mathbf{I}}^{(\mathbf{2})}_{\mathbf{ax}} \\
\mathbf{I}^{(\mathbf{5})}_{\mathbf{lat}} &= \mathbf{L}\overline{\mathbf{I}}^{(\mathbf{4})}_{\mathbf{ax}} \\
\mathbf{I}^{(\mathbf{7})}_{\mathbf{lat}} &= \mathbf{L}\overline{\mathbf{I}}^{(\mathbf{6})}_{\mathbf{ax}} \\
&\vdots,
\end{aligned} \tag{27}$$

with

$$\mathbf{I}_{\mathbf{lat}} = (\mathbf{1} + \mathbf{S}_\perp)(\mathbf{I}^{(\mathbf{1})}_{\mathbf{lat}} + \mathbf{I}^{(\mathbf{3})}_{\mathbf{lat}} + \mathbf{I}^{(\mathbf{5})}_{\mathbf{lat}} + \dots) \tag{28}$$

The attenuation factor for the $\mathbf{K}$ and $\mathbf{L}$ of the scene are respectively in this order κ,κ'. The order of attenuation of

the scene is none other than the largest order κ_{max} among the primitives, which represents the smallest disturbance that want to appear, in this case, this is simply the order of attenuation of the sphere $\kappa_O = 4$, $\kappa'_O = 5$. To achieve this order you have to push the iterations until about the smallest of the scene κ_{min} (the wall in this case) reaches the desired order, knowing that $\kappa_{(f)} = f * \kappa_{(1)}$, $\kappa_{(f)}$ is the order of attenuation for the f^{th} iteration.

then

$$f = \frac{\kappa_{max}}{\kappa_{min}}, \tag{29}$$

with $f \in \mathbb{N}$. In our case $f = \frac{\kappa_O}{\kappa_w}$.

Then the equations are written as:

$$\begin{aligned}\overline{\mathbf{I}}_{ax} = \quad & (\mathbf{1} + (-\overline{\mathbf{C}}^{(0)}\mathbf{K}) + (-\overline{\mathbf{C}}^{(0)}\mathbf{K})^2 + ... \\ & +(-\overline{\mathbf{C}}^{(0)}\mathbf{K})^f)\overline{\mathbf{I}}^{(\mathbf{0})} + O(\epsilon^{f\times\kappa_w})\end{aligned} \tag{30}$$

$$\mathbf{I}_{lat} = (\mathbf{1} + \mathbf{S}_\perp)\mathbf{L}\overline{\mathbf{I}}_{ax} + O(\epsilon^{f\times\kappa'_w}) \tag{31}$$

From there, we can generalize to a complex scene with all the primitive.

4) scene with n_w walls, n_c corners and s spheres: In this case we have a complex scene with all the primitives with n_w,n_c,s are in this order the number of walls , corners and spheres in the scene, we use the equation(29) and (30) to calculate $\overline{\mathbf{I}}_{\mathbf{ax}}$ and $\mathbf{I}_{\mathbf{lat}}$ with this time:

$$\mathbf{K} = \sum_{j=1}^{n_w}\mathbf{K}_{A^*_{w_{(j)}}/A} + \sum_{g=1}^{n_c}\mathbf{K}_{A^*_{c_{(g)}}/A} + \sum_{k=1}^{s}(\mathbf{K}_{A/O_k/A} + \sum_{j=1}^{n_w}(\mathbf{K}_{A/O^*_{k,w_{(j)}}/A} + \mathbf{K}_{A^*_{w_{(j)}}/O_k/A} + \mathbf{K}_{A^*_{w_{(j)}}/O^*_{k,w_{(j)}}/A}) + \sum_{g=1}^{n_c}(\mathbf{K}_{A/O^*_{k,}} \quad _{g)}/A + \mathbf{K}_{A^*_{c_{(g)}}/} \tag{32}$$

with $\mathbf{K}_{A^*_{w_{(j)}}/A}$ describes the effect of the image $A^*_{w_{(j)}}$ to the wall j on the sensor A, $\mathbf{K}_{A^*_{c_{(g)}}/A}$ describes the effect of the image $A^*_{c_{(g)}}$ to the corner g on the sensor A. $\mathbf{K}_{A/O_k/A}$ describes the effect of the sphere O_k on the sensor A, $\mathbf{K}_{A/O^*_{k,w_{(j)}}/A}$, $\mathbf{K}_{A/O^*_{k,c_{(g)}}/A}$ describes the effect of the sphere image $O^*_{k,w_{(j)}}$ to the wall j and the corner g respectively. The same contributions go with $\mathbf{L}$ by summing this time the matrix $\mathbf{L}$ in place of $\mathbf{K}$ on the sensor A.

VI. SIMULATOR AND SIMULATION RESULTS

Based on the reduction scheme presented in [2] and further developed in the previous section, we have developed a simulator under MATLAB that is faster than the simulator based on the boundary element method (BEM) that was already developed in [4]. The aim of the simulator is to calculate the axial and lateral currents of rings sensors present in the scene from the configuration of the positions of objects (sensor,small objects, walls, corners) in the absolute frame. The simulator is divided into two major parts:

1) *Initialization:* That part includes the geometrical and electrical data of different primitives in the scene with the geometrical parameters are the positions and orientations of different in the scene int the absolute frame for some objects (the center of the wall, the intersection for two or three walls for the corner, the center of small object and the center of the sensor), and position of the rings in the relative frame on the sensor. The change of reference frame is done using the homogeneous transformation matrix. The electrical parameters are: the voltage vector of the sensor rings, the conductance matrix vacuum.
2) *Calculating:* This part is responsible for calculating currents of the electrodes from the equations of the analytical model.

A. Experimental conditions:

For all the simulations we have considered the 7 electrodes sensor represented on Fig. 7 (a) with $m = 3$ and $n = 6$. The dimensions of the sensor are: $l = 22cm$, $R = 1cm$ for $\alpha = 0, 1, 2, 3$; $l_{I_1} = 13cm$, $l_{I_2} = l_{I_3} = 2.5cm$. On the electrical side, the water conductivity is $\gamma = 0.04S/m$, while the vector of the voltage is $0V$ for the receivers and $1V$ for the emitter (the tail). We calibrate conductance matrix $\overline{C}^{(0)}$ by calculating it one for all with the BEM in absence of objects :

$$\overline{C}^{(0)} = \frac{\gamma}{100}\begin{pmatrix} 7.6537 & -3.1518 & -2.3179 & -2.1844 \\ -3.1221 & 8.3934 & -3.1998 & -2.0719 \\ -2.2926 & -3.2057 & 7.8032 & -2.3048 \\ -2.1839 & -2.0855 & -2.3333 & 6.6062 \end{pmatrix}$$

Comparison with the BEM simulator was already given in [2] for the case of the sensor with the sphere, so that we will not reproduce it here.

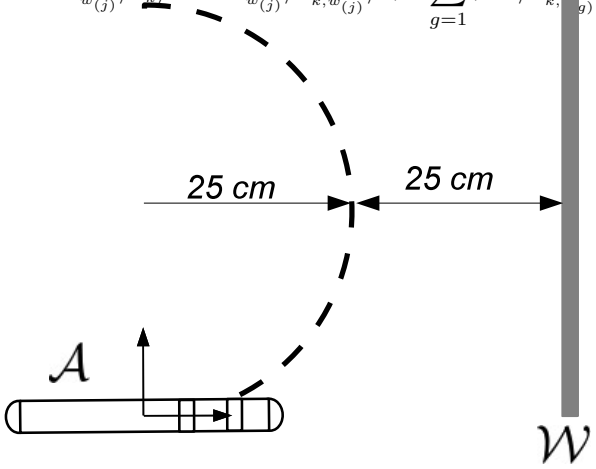

Fig. 5. To test the model for the wall we used a circular trajectory for the sensor. The measurement are compared with both the BEM simulator and the model.

1) The sensor with an aquarium: For this simulation we have a cube-shaped tank of length $L = 1m$, the six faces of the cubes as insulating surfaces and are considered as walls. Each edge is the intersection between two walls and is a corner, there are 12 corners. Each vertex is the intersection of three walls and represents a 3D corner and is the center of central symmetry with respect to the trihedral, there are 8 3D corners. The middle of the aquarium is the origin of the absolute frame. We took a curved path of a semi-circle

form, approaching the wall in front of the sensor as shown on Fig. 7 (b). The trajectory has a radius of 25cm, which the center is remote from the wall of 35cm. In order to qualify the accuracy of the analytical model, the experiment is repeated with the BEM simulator.

Results:

Fig. 8 and Fig. 9 show the currents mesured by the BEM and the model for the semi-circle trajectory. In the BEM, the axial and lateral currents are deduced such as for the ring ϵ_i the axial current is the sum of the electrode currents in each ring, and for the lateral $I_{lat} = I - I_{ax}/k$ (the current is deduced for each electrode). Fig. 8 shows the comparison between the BEM and the simulator based on the analytical model for several iterations in the case of axial current and the absolute error resulting, we see that the greater the number of iterations over the absolute error decreases. The maximum absolute error for the first iteration is $4 \times 10^{-7} A$, while the maximum absolute error for the second iteration does not exceed $2 \times 10^{-7} A$. For the third iteration the average of the diference between this one and the second iteration is 1.7×10^{-9}. We concluded that the signal of the second and third iteration are negligible compared to the useful signal, which is the order of $10^{-4} A$. Fig. 9 shows the comparison between the BEM and the simulator based on the analytical model for several iterations in the case of lateral current and their absolute error. The average difference between the first and second iteration is 1.3×10^{-10}, it is negligible compared to the useful signal, which is the order of $10^{-6} A$.

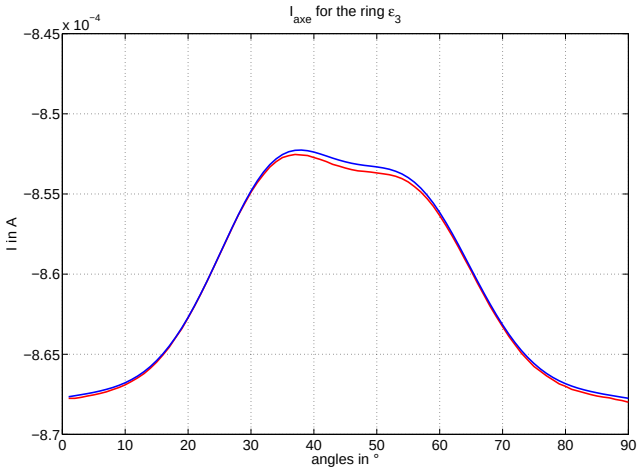

Fig. 6. (a) axial current of the ring ε_3 for each simulation step for the trajectory of the sensor in the tank. (b) absolute error of the sensor axial current for the different iterations.

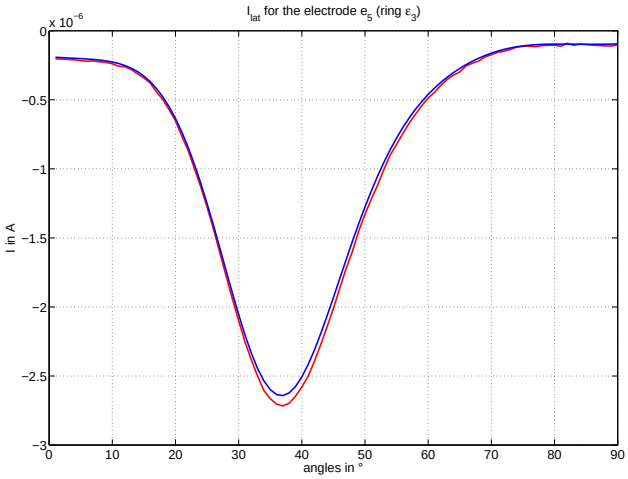

Fig. 7. (a) lateral current of the electrode e_5 of the ring ε_3 for each simulation step for the trajectory of the sensor in the tank. (b) absolute error of the sensor lateral current for the different iterations.

2) The sensor with an aquarium and three spheres: For this simulation we have the same aquarium as before. The middle of the aquarium is the origin of the absolute frame. There are three spheres s_1,s_2,s_3 in the scene with:$a_1 = a_2 = a_3 = 9mm$, s_1,s_3 are insulator $\chi_1 = \chi_3 = -0.5$ and s_2 is conductor $\chi_2 = 1$. Their positions in the absolute frame are $s_1(0.12, -0.1, 0)$,$s_2(-0.4, 0.35, 0)$, $s_3(0.25, 0.33, 0)$. The trajectory of the sensor is divided into three parts as shown in Fig.10, he began his trajectory from position **A**(0.3,-0.35,0) at an angle of 144 to the axis of X. The sensor in a straight line to point **B**(-0.28,0.2,0). Then he began a circular path of $10cm$ radius up to what he reaches the point **C**(-0.22,0.38,0). Finally it runs along the wall with a straight path until the point **D**(0.3,0.38,0). We made two simulations, the first with the spheres in the aquarium and the second with the same path but without the spheres.

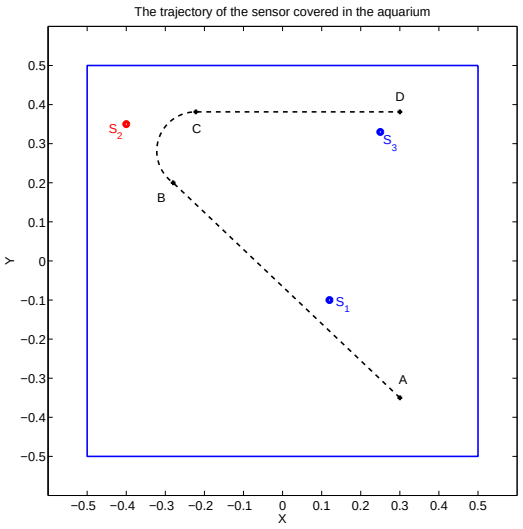

Fig. 8. The trajectory of the sensor covered in the aquarium

Results:

Fig. 11 shows the currents obtained by the BEM and the simulator for the trajectory of the ring ϵ_3 shown in Fig. 10. The error for various iterations changes with the trajectory: at point **A** the error is larger for currents with multiple iterations and it is normal because the electrode tail (the emitter ϵ_0) is too close to the wall, the error is due to the limit of validity of the model. From **A** to **B** can be seen that the increased number of iterations does not significantly influence the results of the error, because the sensor approaches the center of the aquarium, making the influence of different wall very small. From **B** to **C** the error current for several iterations increases until it reaches its maximum at the point **M**, because the ring being too close to the wall (fig. 10). It is beyond the range of validity of the model (distance $< 10cm$). So, to the limit of validity of the model (too close to the wall or corner), the change is felt and the error increases with the addition of iteration. From **C** to **D** the greater the number of iterations over the error decreases (knowing that from the third iteration, the difference between each two successive iterations become negligible in the range of 10^{-11}A), with the distance between the ring and the wall being greater than 10 cm. Approaching the point **D** the error increases due to the influence of the corner, which is double of the wall (i.e. the range of validity of the corner is bigger than the wall).

The errors are not linked only to the range of validity of the model but also to the BEM. Errors in the BEM, are due to the calculation of the conductance vacuum $\overline{C}^{(0)}$. The notion of the void in this case means to calculate the conductance at the center of a large aquarium ($5m$ in our case with a specific mesh (30 mesh per wall)). Errors are due to the rather limited number of mesh for walls (reaching the maximum number that can take into account the program of the BEM).

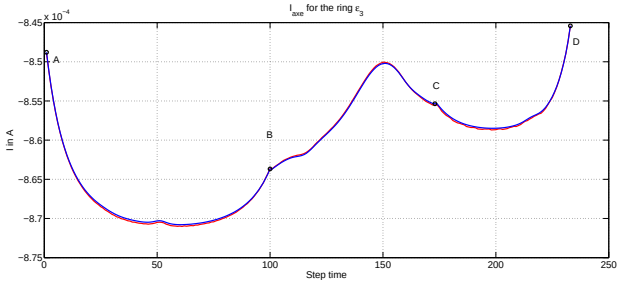

Fig. 9. (a) axial current of the ring ε_3 for each simulation step for the trajectory of the sensor in the tank in the presence of spheres. (b) absolute error of the sensor in the aquarium in the presence of spheres for the different iterations.

The fig.12 (a) shows the comparison between the axial current with and without spheres. Note that the influence of the spheres is embedded in the signal from the aquarium, and we can separate the two with difficulty, this is due to the order of magnitude of the currents caused by the presence of spheres in the scene, which is smaller than the order of magnitude for the walls.

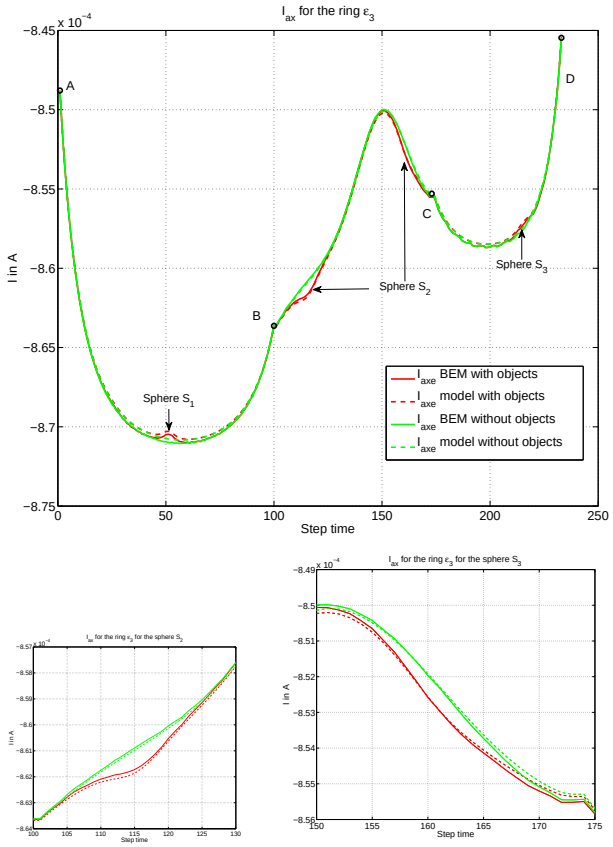

Fig. 10. (a) comparison between the axial current of the ring ε_3 for each simulation step for the trajectory of the sensor in the tank in the presence of spheres and without the spheres. (b) absolute error of the axial current in the aquarium without the spheres for the different iterations.

Comparing the error of the trajectory in the aquarium

with sphere (Fig. 11(b)) and without sphere (Fig. 12(b)) we see that the errors for the different iterations are practically the same in both cases. We concluded that the presence of small objects does not influence the errors obtained for the various iterations since the magnitude is smaller than that of the walls.

Fig.13 (a) shows the comparison between the lateral current with and without spheres. Note that unlike the axial current the influence of spheres S_2 and $S-3$ are apparent because they are currents in the range of 10^{-7} and for the influence of the walls is 10^{-6}.In fig.13 (b) the errors do not improve greatly with the addition of iterations, the average diference between the first and the second iteration is 1.03×10^{-10}. We conclude that for the lateral currents , the iterations are in the range of negligible.

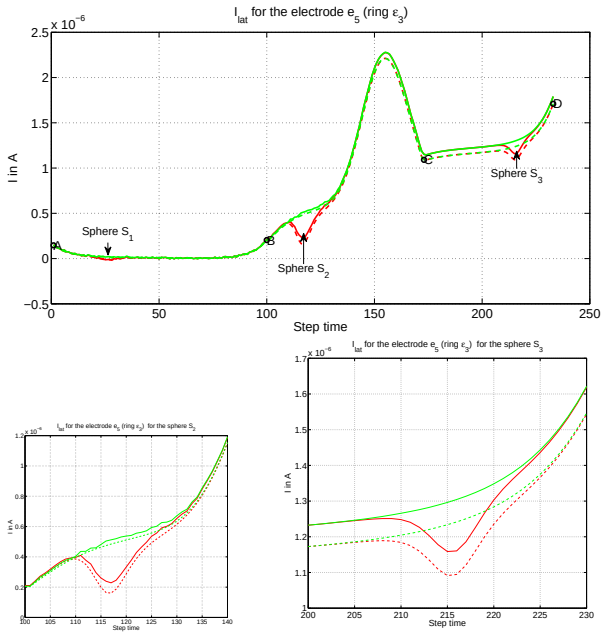

Fig. 11. (a) comparison between the lateral current of the electrode e_5 for each simulation step for the trajectory of the sensor in the tank in the presence of spheres and without the spheres. (b) absolute error of the lateral current in the aquarium with and without the spheres for the different iterations.

Comparing the computation time for three simulations with the BEM and the simulator based on the model, we obtain time for the simulator in order are: $35.09sec$, $51.5sec.65sec$, and for BEM $32259sec$, $320230sec.343790sec$, with a mean relative error between the two is less than 3 %. We can conclude that the simulator provides a good compromise between speed and accuracy for the calculated currents.

VII. MULTI-AGENT

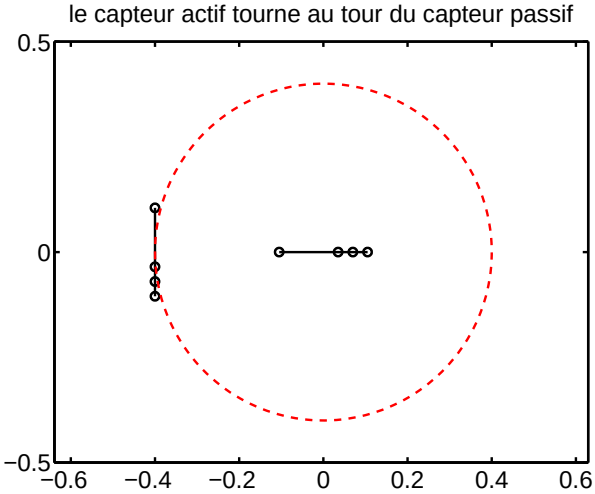

Fig. 12. Trajectory for multiagents simulation

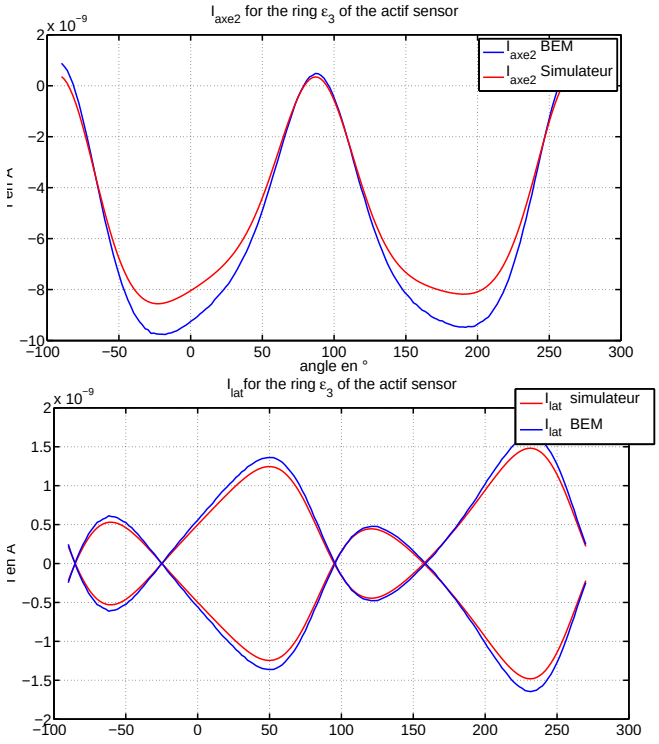

Fig. 13. The axial and lateral current for the active agent

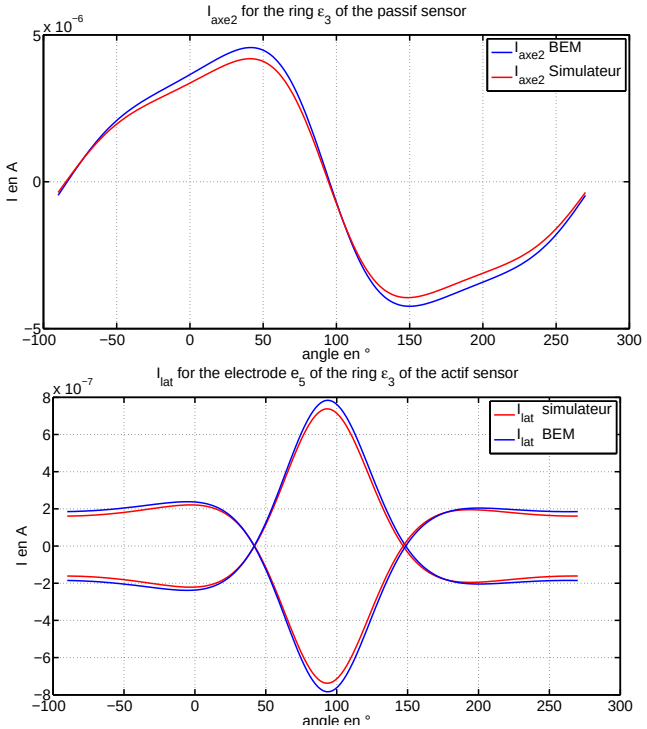

Fig. 14. The axial and lateral current for the passif agent

VIII. Conclusion

As demonstrated in previous section, the analytical reduction scheme for the wall is in good agreement with the reference BEM. We have presented an extension of the model for electrolocation based on the method of successive reflections for different primitives and complex scenes allowing navigation in an environment constrained by the walls. Based on thsi model we have developed a simulator under MATLAB that is faster than the simulator based on the boundary element method (BEM) with a good compromise between speed and accuracy for the calculated currents.

References

[1] H.W. Lissmann and K.E. Machin. The mechanism of object location in gymnarchus niloticus and similar fish. *J.Exp.Biol.*, 35:451–486, 1958.

[2] F. Boyer, P.B. Gossiaux, B. Jawad, V. Lebastard, and M. Porez. Model for a sensor inspired by electric fish. *IEEE transactions on robotics*, 2011.

[3] J.D. Jackson. *Classical Electrodynamics*. John Wiley and Sons, 1962.

[4] Mathieu. papier sur la bem.